Published in final edited form as:
Clin Exp Pharmacol Physiol. 2010 August ; 37(8): 852–861. doi:10.1111/j.1440-1681.2010.05396.x.

Functional impact of the hyperpolarization-activated current upon the excitability of myelinated A-type vagal afferents neurons in rat

Yu-Hong Zhou[*,1], **Li-Hua Sun**[*,1], **Zhen-Hong Liu**[*], **Guixue Bu**[‡], **Xiao-Ping Pang**[*], **Shi-Chao Sun**[*], **Guo-Fen Qiao**[*,†], **Bai-Yan Li**[*,§], and **John H Schild**[§]

[*]Department of Pharmacology, Harbin Medical University, Harbin, China

[†]State-Province Key Laboratories of Biomedicine Pharmaceutics, Harbin Medical University, Harbin, China

[‡]Department of Radiology, Indiana University Hospital, Indianapolis, USA

[§]Department of Biomedical Engineering, Purdue School of Engineering and Technology, Indiana University Purdue University Indianapolis, Indianapolis, USA

Summary

1. The hyperpolarization induced cation selective current, I_h, is widely observed in peripheral sensory neurons of the vagal and dorsal root ganglia but the peak magnitude as well as the voltage and time dependent properties of this current vary widely across afferent fiber type.

2. Through patch clamp study of isolated rat vagal ganglion neurons identified as myelinated A-type afferents we establish a compendium of functional correlates between changes in membrane potential and the dynamic discharge properties of these sensory neurons as a result of the controlled recruitment of I_h using the current clamp technique.

3. Two robust observations in response to hyperpolarizing step currents: 1) upon initiation of the negative step current there was a rapid hyperpolarization of membrane potential followed by a depolarizing sag (DVS) toward a plateau in membrane potential as a result of steady state recruitment of I_h, and 2) upon termination of the negative step current there was a rapid return to the pretest resting membrane potential that often led to spontaneous action potential discharge. These data strongly correlated ($r^2 > 0.9$) with a broad compendium of dynamic discharge characteristics in these A-type VGN.

4. In response to depolarizing step currents of increasing magnitude the discharge frequency of the A-type VGN summarize reliably responded with increases in the rate of sustained repetitive discharge. Upon termination of the depolarizing step current there was a post excitatory membrane hyperpolarization with a magnitude that strongly correlated with action potential discharge rate ($r^2 > 0.9$).

5. Application of the selective HCN channel blockers 10 μM ZD7288 or 1.0 mM CsCl abolished I_h and all of the aforementioned functional correlates in addition to reducing the excitability of the A-type VGN to step depolarizing currents.

Correspondence: Dr. G-F Qiao, MD & PhD, Department of Pharmacology, Harbin Medical University, Bao-Jian Road 157, Harbin 150081, China; Phone: 86-451-8667-1354; qiaogf88@yahoo.com.cn.
[1]Authors contributed equally to this work

6. As evidence is growing that the HCN channel current may represent a valid target for pharmacological intervention such quantitative relationships could potentially help guide the molecular or chemical modification of HCN channel gating properties to effect a particular outcome in VGN discharge properties. Ideally, well beyond merely selective blockade of a particular HCN channel subtype.

Keywords

Hyperpolarization-activated current (I_h); HCN channel; neuronal excitability

Introduction

The hyperpolarization-activated current is an inward current carried by sodium and potassium ions through hyperpolarization-activated cyclic nucleotide gated (HCN) channels.(19;35) HCN channels open in a voltage dependent manner at hyperpolarized membrane potentials producing a whole cell current with at least 2nd order voltage-dependent activation characteristics with time constants ranging from a few hundred milliseconds to over one second. HCN channels close upon depolarization and do not exhibit voltage- or time-dependent inactivation. Four distinct subunits, HCN1-4, can give rise to a whole cell I_h ion channel current that has been shown to contribute in setting resting membrane potential and modulation of cell excitability but paradoxically can do so as either pro- or anti-excitatory depending upon spatial and temporal expression of particular HCN channel subtypes as observed in both the central and peripheral nervous systems.(1;3;7;25) The reasons for such functional heterogeneity are not well understood but may be a consequence of differences in kinetics of activation, deactivation and modulatory capacity of cAMP across all four channel subtypes. HCN channel dysfunction has been shown to be associated with a variety of clinical pathologies including cardiac dysrhythmias, ataxia, absence epilepsy and neuropathic pain syndromes.(4;12;18;21;29) Recent cloning of HCN isoforms raises the possibility for development of selective blockers or modulators of HCN channel function, perhaps with a level of specificity that extends not only to channel subtype but also through to a particular pathophysiology that may be associated with noted transformations in the whole cell I_h.(12;25;29)

Recently, comprehensive electrophysiological and immunohistochemical studies have consistently presented evidence that HCN1 channels make a significant contribution to the whole cell I_h in visceral neurons of the vagal ganglia (VGN) and somatic sensory neurons of the DRG, especially in what are believed to be myelinated, A-type mechanosensitive afferents.(7;17;22;31;34) A study by Doan et al. (2004) presented further evidence that HCN1 was absent from unmyelinated C-type vagal afferent neurons and mechanosensitive nerve terminals, and although HCN2 and HCN4 were present in receptor terminals of both myelinated A-type and unmyelinated C-type fibers the immunoreactivity was somewhat less apparent. Nevertheless, mRNA and optical evidence for protein expression in visceral and somatic afferents have been reported for all four subtypes of HCN channels. Although there appears to be general agreement concerning the expression of HCN1 in myelinated afferents, there are conflicting observations concerning expression of HCN2, HCN3 and HCN4 between myelinated and unmyelinated afferents and intriguing functional differences between classes of somatic and visceral afferents.(7;17;22;31;33;34) It is generally accepted that application of low concentrations of ZD7288 (1 – 10 μM), an antagonist of all four HCN channel subtypes, hyperpolarizes resting membrane potential of both visceral and somatic sensory neurons, albeit to a lesser extent in lightly myelinated and unmyelinated afferents.(6;9;17;21) However, these reports and others in the literature differ in that ZD7288 elevates the excitability of myelinated A-type visceral afferents but that excitability

decreases with the loss of the I_h current in somatic, large diameter myelinated A-type afferents. The biophysical basis for such stark functional differences remains unknown.

The overarching objective of this study is to establish functional correlates between the magnitude and time course of the recruitment of the I_h current and the dynamic discharge properties of adult rat vagal ganglion neurons (VGN) that have been functionally classified as myelinated A-type afferents. Using the patch clamp technique to apply a suite of current clamp protocols we have made the following observations. First, there exists a strong correlation ($r^2 > 0.9$) between the peak magnitude and time course of the I_h current and several measures of VGN excitability in response to depolarizing step currents. Second, following an epoch of repetitive discharge that is abruptly terminated upon completion of a 400 – 1000 msec current step there is a period of post excitatory membrane hyperpolarization of a magnitude and time course that again strongly correlates ($r^2 > 0.9$) with the magnitude and time course of the I_h current and the sustained rated of VGN discharge. Third, following the termination of a hyperpolarizing current step there is a rebound in membrane potential toward the starting resting membrane potential that results in spontaneous action potential discharge of rapidity that strongly correlates ($r^2 > 0.9$) with the magnitude and time course of the I_h current. All of these functional characteristics are eliminated with the extracellular application of 10 μM ZD7288 or 1 mM CsCl in addition to bringing about a marked diminution in VGN excitability to depolarizing step currents. In a subset of experiments using female rats, we confirm that these functional correlates are also present, albeit to a lesser extent, in a population of gender specific myelinated Ah-type vagal afferents recently described by our group.(14;24) Collectively, these data provide the basis for a comprehensive explanation of several unique roles for the I_h current in effecting the dynamic discharge characteristics of myelinated vagal afferents beyond that which can be solely attributed to the well recognized contribution of I_h in setting resting membrane potential.

Materials and Methods

Standard cellular electrophysiological methods were carried out using the patch clamp technique to quantify the functional impact the HCN channel mediated I_h current has upon the repetitive discharge characteristics of isolated vagal afferent neurons (VGN). In all recordings VGN were reliably identified as one of three distinct subtype of visceral afferent, namely, myelinated A-type, myelinated Ah-type or unmyelinated C-type using previously developed classification methods [12, 13].

Isolation of vagal afferent neurons

Adult male Sprague Dawley rats (n = 22, 200–300 g) were used in the preparation of isolated VGN. The bilateral dissection of the vagal ganglia, enzymatic digestion, plating and short term culture of the dispersed VGN have been described elsewhere [10, 11]. Briefly, surgical dissection of the vagal ganglia was carried out under stereomicroscopy (×40). The vagal ganglia was immediately placed in chilled support medium containing 90 ml DME-F-12 medium (Sigma), 5 ml Fetal Bovine Serum (HyClone), 1.0 ml Penicillin-Streptomycin (Invitrogen) and 100 μM of MITO + Serum Extender (BD Biosciences). Following the addition of 10 units/ml of Papain (Sigma) the ganglia were incubated at 37 °C for 20 min. The ganglia were then transferred to fresh support medium containing 1.0 mg/ml type II Collagenase and 2.5 mg/ml Dispase (Worthington Biochemical) and incubated at 37°C for additional 30 min. A mechanical dispersion of the digested tissue was carried out using polished Pasteur pipettes. The enzyme solution was replaced with fresh support medium. The VGN were plated on to poly-D-lysine coated glass cover slips and incubated for at least 2 hours prior to electrophysiological study. In a subset of experiments VGN from female Sprague Dawley rats (n = 7, ~200 g) were prepared in an identical manner. All animal use

protocols were approved by the Institutional Animal Care and Use Committees of the School of Medical Science, Harbin Medical University and Purdue School of Science, IUPUI.

Electrophysiological solutions

For AP recordings, the intracellular solution consisted of (mM) 10 NaCl, 50 KCl, 50 K_2SO_4, 5.0 $MgCl_2$, and 10.0 HEPES with the pH adjusted to 7.25 using 1N KOH. Immediately prior to filling the patch pipettes 2.0 mM Mg-ATP (Sigma) and 2.0 mM Na-GTP 2.0 mM (Sigma) along with were added to the pipette solution along with 4.0 mM Bapta-Na and 0.25 mM $CaCl_2$ for a final buffered $[Ca^{2+}]_i$ of 100 nM. The extracellular recording solution consisted of (mM): 137 NaCl, 5.4 KCl, 1.0 $MgCl_2$, 2.0 $CaCl_2$, 10 glucose, 10 *N*-2-hydroxyethylpiperazine-*N'*-2-ethanesulfonic acid (HEPES) with pH adjusted to 7.30–7.35 using 1N NaOH. The osmolarity of the extracellular and intracellular solutions was adjusted to 310 – 315 and 290 – 295, respectively, using D-Manitol (Sigma).

Drugs and Chemicals

A 100 μM of stock solution of the HCN channel antagonist ZD7288 (Tocris) was prepared using extracellular recording solution which was diluted to 10 μM just prior to study. Bath application of ZD7288 was carried out at a rate of ~1 ml/min for a period of at least 10 min prior to test recording to ensure the full effectiveness of this agent. A 1 mM stock of CsCl (Sigma) was also prepared and bath applied in a similar manner.

Electrophysiological techniques

Whole-cell patch recordings were carried out using the Axopatch 200B or MultiClamp 700A amplifier (Axon Instruments). Borosilicate glass pipettes (Sutter Instruments) were pulled and polished down to 1.5 – 2.4 MΩ as measured in action potential (AP) recording solution (see below). Following the formation of a giga-ohm seal the pipette capacitance was compensated. The total cell capacitance (30 – 40 pF) and electrode access resistance (3 – 5 MΩ) were also compensated and generally to within 60–80%. All patch experiments were conducted at room temperatures (22–23 °C). Data traces were low pass filtered to 10 KHz and digitized at 50 KHz using pCLAMP 9.0 or 10.2 and the Digidata 1322A or 1440A (Molecular Devices) operating on a PC platform.

Three distinct experimental protocols were carried out in current clamp mode. First, each cell was hyperpolarized using current magnitudes ranging from −80 to −120 pA for 400 msec to quantify the magnitude and time course of the hyperpolarization induced depolarizing voltage sag (DVS) in membrane potential as a result of recruitment of the inward conducting HCN channel currents. Second, a single somatic AP was elicited by applying a brief (< 500 μsec) suprathreshold current pulse through the patch electrode. Third, depolarizing current steps (50 – 300 pA) ranging from 500 – 1000 msec were applied through the patch electrode from a reference potential of ~−60 mV. This adjustment from the cell's intrinsic resting membrane potential was carried out to assess the capacity of the cell under study for sustained, repetitive discharge starting from a consistent membrane potential and therefore, presumably, a more consistent availability of voltage gated ion channels.

Identification neuronal cell type

Enzymatic dispersion separates the cell body from its axon and thus afferent cell type can not be classified according to a measure of fiber conduction velocity (CV). Using an intact ganglion preparation that allows for measure of fiber CV, we recently developed a reliable and robust methodology for classifying an isolated VGN as either a myelinated A-type,

myelinated Ah-type or an unmyelinated C-type VGN.(15;16) Here, we demonstrated that three measures of the AP wave form, i.e. the AP firing threshold (APFT), the AP upstroke velocity measured at 50% peak-to-peak excursion (UV_{APD50}) and the AP down stroke velocity (DV_{APD50}) uniquely clustered into three statistically distinct populations according to whether a cell is a myelinated A- or Ah-type or an unmyelinated C-type VGN. Following classification of cell type the electrophysiological traces and AP waveform measures were further analyzed using Clampfit (Molecular Devices). Pooled statistics were calculated using Excel (Microsoft) with measures expressed as mean ± standard deviation (SD). Comparisons across population samples were carried out using either a student's t-test or ANOVA as indicated. Data populations exhibiting an overlap of 5% or less were considered to be statistically different.

Results

The average resting membrane potential (RMP) of all cells in this study was −64 ± 5 mV (n = 75), over a range of −59 to −78 mV. 47 cells were classified as myelinated A-type, 6 classified as myelinated Ah-type and 22 classified as unmyelinated C-type with no statistical difference noted in the RMP across the three populations of neuronal subtypes.

Hyperpolarizing currents evoke a depolarizing voltage sag in myelinated A-type VGN

In response to a single suprathreshold depolarizing current pulse all myelinated A-type VGN (n = 47) exhibited narrow AP wave shapes (0.81 ± 0.1 msec) with an UV_{APD50} typically in excess of 300 mV/msec (394 ± 55 mV/msec). Although presenting relatively uniform wave shape characteristics (Figs. 1A, 1D and 1G are but three examples) depolarizing current steps of the same 150 pA magnitude and duration elicited markedly different rates of sustained discharge of 31 Hz, 47 Hz and 109 Hz (Figs. 1B, 1E and 1H, respectively). Interestingly, cells with elevated rates of discharge exhibited a prominent post excitatory membrane hyperpolarization (PEMH) immediately upon termination of the current step while myelinated VGN that were less excitable tended to have a very modest or entirely absent PEMH (note ▲ at the end of each of the traces in Figs. 1B, 1E and 1H). Application of a −120 pA for 400 msec hyperpolarized the cell membrane and brought about a depolarizing voltage sag (DVS) but with marked differences in peak magnitude and time course of the DVS. As with the three example VGN presented here, those cells that were less excitable exhibited a modest peak hyperpolarization and DVS (Figs. 1A, 1B and 1C). As the excitability of the VGN tended to increase the same −120 pA revealed an ever increasing peak hyperpolarization potential and a more prominent DVS (note ● and rate of the DVS toward a plateau potential across Figs. 1C, 1F and 1I). Likewise, release of the −120 pA hyperpolarizing current tended to bring about a more pronounced rebound excitation as the membrane recovered toward resting membrane potential (note AP at the end of the hyperpolarized traces in Figs. 1C, 1F and 1I).

Correlation between myelinated A-type VGN discharge properties and DVS

For the three cells presented in Figure 1 there appeared to be a positive trend toward an increased magnitude and time course of the PEMH, the peak hyperpolarization and the DVS for those VGN exhibiting increased in response to step depolarizing currents. Here, a large sample (n = 47) of VGN were investigated through a sequential application of the same three testing protocols presented in Figure 1. From this data set six functionally distinct electrophysiological measures of VGN membrane properties were carried out: 1) steady state AP firing frequency (APFF) in response to a 1000 msec, 150 pA step depolarizing current, 2) resting membrane potential (RMP) in the presence of 0 pA of electrode current, 3) AP firing threshold (APFT) measured as the membrane potential corresponding to a ×10 change in the time derivative of membrane potential, 4) the maximum AP upstroke velocity

(UV_{MAX}) measured as the peak positive time derivative of membrane potential, 5) the maximum AP down stroke velocity (DV_{MAX}) measured as the peak negative time derivative of membrane potential and 6) the width of the AP measured at 50% of the peak-to-peak amplitude (APD_{50}). Each of these pooled measures was correlated with the peak magnitude of membrane hyperpolarization leading to the depolarizing voltage sag (DVS) in response to a 400 msec, −120 pA current step from RMP. Remarkably, each of these measures strongly correlated with the magnitude and time course of the DVS (Fig. 2).

Post excitatory membrane hyperpolarization correlates with discharge frequency in A-type VGN

All myelinated A-type VGN exhibited PEMH upon termination of stimulus current induced repetitive discharge (Fig. 1, ▲) albeit with differences in peak magnitude and time course of recovery to RMP. In a subset of VGN identified as A-type (n = 6), three 400 msec depolarizing step currents of 50, 100 and 150 pA were applied at an interval of 5 sec to ensure complete recovery to the starting RMP and lessen the likelihood of cumulative effects of repetitive discharge upon intracellular characteristics. As expected, increasing current magnitudes brought about more elevated rates of repetitive discharge: 25.5 ±16.2 Hz @ 50 pA, 42.6 ± 21.3 @ 100 pA and 58.8 ± 26.1 Hz @ 150 pA (Fig. 3). Interestingly, the average peak magnitude of the PEMH trended toward more negative potentials with increasing stimulus current: −66.2 ± 5.2 mV @ 50 pA, −71.4 ± 4.7 at 100 pA and −76.8 ± 4.0 mV @ 150 pA (Fig. 3, note ▲ upon termination of repetitive discharge). No statistically significant differences in measures of dynamic discharge characteristics such as peak AP height or peak of the afterhyperpolarization were observed. Therefore, the most apparent impact of an increasing stimulus current magnitude upon VGN membrane dynamics may be most comprehensively assessed by measure of repetitive discharge rate. In that regard the peak PEMH was found to be strongly correlated with the steady state APFF ($r^2 = 0.979$).

Rebound discharge as a function of the magnitude and time course of DVS in A-type VGN

Following the termination of the −120 pA hyperpolarizing current step all myelinated A-type VGN tended to generate an AP as membrane potential rebounded toward the RMP (Fig. 1C, 1F, 1I). However, this occurred with markedly different trajectories toward AP discharge. Therefore the hypothesis was put forth that the peak magnitude and time course of the DVS may be influencing the rate of rebound discharge. A subset VGN were identified as myelinated A-type (n = 6) based upon measures of AP wave shape characteristics with an average APFF of 54.6 ± 12.6 Hz in response to a 150 pA step current. Following classification of the VGN as a myelinated A-type 400 msec hyperpolarizing current steps from −70 to −120 pA in −10 pA increments were applied through the patch electrode at an interval of one step each 5 sec. This extended test interval ensured the VGN recovered to the initial RMP before the next hyperpolarizing current injection. As expected, more negative step currents brought about an ever increasing magnitude of the peak hyperpolarization as well as more negative membrane potentials at the end of the DVS (Fig. 4). Interestingly, in the presence of nearly twice the hyperpolarizing current magnitude the membrane potential along the plateau of the DVS remained within a range of ~10 mV. Furthermore, the time course of the DVS through to the plateau in membrane potential near the end of the pulse was strongly correlated with the peak hyperpolarization; first order time constants of 83.2 ± 22.4 msec @ −70 pA, 75.8 ± 18.6 msec @ −80 pA, 70.5 ± 17.1 msec @ −90 pA, 66.1 ± 16.9 msec @ −100 pA, 49.8 ± 13.7 msec @ −110 pA, and 43.8 ± 12.2 msec @ −120 pA followed a linear trend line with an r^2 value of 0.958. Upon release of the hyperpolarizing current the membrane potential rebounded toward the starting RMP which often led to spontaneous generation of one or more AP (Figs. 5A and 5B). Despite the relatively similar plateau membrane potential the time delay between release of the hyperpolarizing current and the measured APFT for spontaneous AP discharge shortened and the maximum

derivative of membrane potential increased as the peak magnitude of the DVS increased (Figs. 5C, 5D and Table 1). Alignment of these spontaneous AP according to the measured time point of APFT revealed an inverse relationship between DVS magnitude and the duration of the spontaneous AP.

Impact of ZD7288 and CsCl on DVS and excitability of A-type VGN

The magnitude and time course of the hyperpolarizing current induced DVS exhibited all the functional hallmarks of a whole cell I_h type current arising from membrane bound hyperpolarization-activated, cyclic nucleotide-gated cation channels (HCN). Therefore, 10 μM of ZD7288 a selective antagonist of the HCN channel subtypes HCN1, HCN2 and HCN4 was applied to a subset of VGN identified as myelinated A-type (n = 5). Control protocols consisted of a 1000 msec, 150 pA current step from RMP to quantify the repetitive discharge characteristics of the particular A-type VGN under study followed by a 400 msec, −120 pA current step to quantify the magnitude and time course of the DVS. In response to the 150 pA depolarizing current step the cells exhibited an average APFF of 55 ± 22 Hz and peak PEMH of −72.6 ± 6.7 mV (Fig. 6A). In response to the −120 pA hyperpolarizing current step the cells exhibited an average peak membrane hyperpolarization of 116 ± 22 mV which brought about a DVS that plateaued to an average membrane potential of 85.2 ± 5.8 mV. In all cells, termination of the 400 msec −120 pA pulse resulted in a rapid rebound in membrane potential and generation of at least one spontaneous AP (Fig. 6B). These two protocols were repeated following an ~10 min bath application of 10 μM ZD7288. Application of this selective HCN channel antagonist significantly reduced membrane potential from an average of −62.9 ± 3.24 mV to −69.3 ± 4.18 mV ($p < 0.01$). Application of a small (10 – 50 pA) background depolarizing current returned the RMP of the cell to near the −62 mV average (−64.0 ± 3.6 mV). The same depolarizing current step failed to elicit sustained repetitive discharge but rather irregular patterns of burst AP discharge which dropped the average APFF over the 1000 msec current step down to 6.2 ± 2.1 Hz. The prominent PEMH was now effectively absent and thus following termination of the depolarizing step current membrane potential fell to a membrane potential (−65.8 ± 3.2 mV) that was not statistically different from the pretest RMP following baseline adjustment. In the presence of ZD7288 there was a significant increase in the peak hyperpolarization potential from the control of 116 ± 22 mV down to 131 ± 17 mV and the DVS was completely abolished. Interestingly, even though the membrane potential was substantially more hyperpolarized in the presence of ZD7288, release of the −120 pA current revealed a markedly slower rebound toward the starting RMP and a complete lack of spontaneous AP discharge (Fig. 6B). As low concentrations of extracellular cesium are known to have a similar blocking effect upon these HCN channel subtypes, the same protocols were repeated in a subset of myelinated A-type VGN (n = 5) but with the test recordings consisting of bath application of 1 mM CsCl. Although there were modest differences between the effectiveness of 10 μM ZD7288 and 1 mM CsCl in limiting cell excitability and the DVS these did not rise to the level of statistical significance.

Comparative analysis of DVS, PEMH and rebound excitation in Ah-type and C-type VGN

Our lab has recently identified a unique subpopulation of myelinated vagal afferents that are found far more frequently in female than male rats.(14) Termed Ah-type because of a prominent hump during the repolarization phase of the AP we sought to determine if Ah-type VGN also exhibited a hyperpolarizing induced current and whether it functioned in a manner similar to that observed in A-type VGN. A small cohort of age matched female rats were used for study of a sample of VGN identified as myelinated Ah-type (Fig. 7A, $n = 6$). In response to 150 pA step depolarizing currents Ah-type VGN exhibited repetitive discharge albeit at a previously confirmed reduced level of excitability but still sufficient to elicit a prominent PEMH (Fig. 7B, as indicated by ▲). A −120 pA current step brought

about a DVS that was not markedly different than that observed in A-type VGN which was also followed by spontaneous generation of one or more AP (Fig. 7B). As with A-type VGN, application of 10 μM of ZD7288 reduced the APFF, PEMH, DVS and generation of spontaneous AP discharge following release of the hyperpolarizing current stimulus (data not shown).

These same electrophysiological protocols were carried out using a population of VGN identified as unmyelinated C-types (n = 22, Fig. 7C). As expected, C-type VGN were far less responsive to step depolarizations with 19 cells producing a single AP, 2 cells exhibiting a short AP burst and one with repetitive discharge of less than 5 Hz (Fig. 7D). None of the C-type VGN exhibited an obvious hyperpolarization current-induced DVS. Likewise, none of the other functional characteristics of the I_h current seen in myelinated A- and Ah-type VGN was observed in C-type VGN (Fig. 7D).

Discussion

This study has classified a broad range of functional correlates between the magnitude and time course in the HCN channel mediated recruitment of I_h and the dynamic discharge properties of adult rat VGN identified as myelinated A-type afferents. In broad terms, those A-type VGN with the most negative peak membrane potential and DVS in response to −120 pA step currents from an adjusted RMP of approximately −60 mV exhibited the highest rates of discharge in response to 150 pA step currents from this same adjusted RMP (Figs. 1 and 2A). Likewise, DVS and excitability were strong indicators ($r^2 > 0.9$) of several functional characteristics such as the extent to which membrane potential hyperpolarized (post-excitatory membrane hyperpolarization, PEMH) following termination of a 150 pA step current (Fig. 3) and the likelihood of spontaneous AP discharge following termination of hyperpolarizing step currents (Fig. 5). In the presence of 10 μM ZD7288 or 1 mM CsCl, chemicals known to block the HCN channel ionic current, there was a significant hyperpolarization in membrane potential and a complete abolishment of DVS, PEMH and rebound excitation (Fig. 6). In a subset of experiments using female rats, we confirm that these functional correlates are also present, albeit to a lesser extent, in a population of gender specific myelinated Ah-type vagal afferents recently described by our group (Figs. 7A, 7B).(14;24) Furthermore, these functional characteristics were essentially absent from VGN identified as unmyelinated, C-type afferents (Figs. 7C, 7D).

Evidence that DVS, PEMH and rebound excitation result from an HCN channel mediated current

There is considerable support in the literature concerning the selective blocking of I_h by low μM concentrations of ZD7288 and low mM concentrations of CsCl and that these chemicals are antagonists for all four identified subtypes of the HCN channels that contribute to the I_h.(34) For sensory neurons from the vagal and dorsal root ganglia there is considerable agreement that 1) an inward I_h current is active at RMP with application of ZD7288 or CsCl resulting in membrane hyperpolarization and 2) for neurons identified as mechanosensory myelinated A-type (either by AP characteristics, cell diameter, or ion channel expression) the majority of the I_h is believed to be the result of HCN1 channel currents.(6;7;9;21;22;33;34) Although our data lacks the resolution to conclusively identify an HCN1 channel current as the source of the ionic flux that brings about the DVS in response to hyperpolarizing current steps, the similar effects of ZD7288 and CsCl upon membrane potential and the DVS lead us to conclude that these biophysical characteristics result from the I_h present in VGN.(6;7)

There are three distinguishing features of the DVS that results in response to hyperpolarizing step currents from RMP: 1) the peak negative response in membrane voltage, 2) the

asymptotic transition to a more depolarized plateau in membrane potential and 3) the time course of the transition between these two features (Figs. 1, 4 and Table 1). Our data clearly showed a strong correlation ($r^2 > 0.9$) between the peak negative response of the DVS and a broad range in functional characteristics of VGN identified as myelinated A-type (Fig. 2). This is not, however, an indication that the peak magnitude of I_h, as would be revealed under conditions of voltage clamp, also correlates with these same functional characteristics. Our comprehensive examination of cell excitability and AP characteristics suggests a coordination in the functional expression of other voltage gated ion channel subtypes and the functional role of I_h in bringing about, for example, PEMH and rebound excitation. As the peak response of the DVS trended toward more negative membrane potentials, the AP waveforms from corresponding A-type VGN exhibited a more negative APFT, a more positive UV_{MAX}, a more negative DV_{MAX} and a more narrow AP waveform as measured at the APD_{50} (Fig. 2). A previous mathematical model of A-type VGN discharge demonstrated that such a trend in AP characteristics could arise from a coordinated increase in the TTX-sensitive Na^+ and the 4-AP sensitive K^+ currents, which would also bring about an elevated maximum discharge rate.(27;28) While I_h can be reasonably assumed to bring about DVS, the broad array of dynamic discharge characteristics of myelinated A-type VGN is most likely the result of a coordinated expression of the HCN channel subtype(s) responsible for I_h and the balance of voltage gated ion channels present in these cells.(26)

Peak and plateau response of the DVS in response to hyperpolarizing currents of varying magnitude—An increase in the peak negative response of the DVS could be interpreted as an indication the cell has a the same or even a smaller magnitude of I_h. Evidence for this can be found in the correlation between RMP and peak DVS (Fig. 2B) which is suggestive of an increased resistance of the cell membrane with decreasing RMP potentially as the result of a smaller net I_h. As neuronal input resistance increases RMP generally trends toward the reversal potential for K^+ ions (E_K) which is about −87 mV in our preparations. Therefore, the combination of a smaller I_h and increased input resistance could explain the more negative response of the peak DVS in A-type VGN with a more negative RMP (Fig. 2B, $r^2 = 0.98$). This observation is consistent with the IV plot of averaged (n = 5) peak DVS and plateau membrane potential across hyperpolarizing current steps from −120 to −70 pA where the averaged peak DVS varied by nearly 50 mV but the plateau potential differed by just under 10 mV (Fig. 4). This suggests that while there may be considerable variability in the activation time constant for I_h in similar sized cells, as A-type VGN often are, the steady state magnitude of the I_h current does not vary by more than approximately 50% over the range of plateau voltages brought about by the hyperpolarizing step current injections (i.e −85 to −78 mV). These conclusions regarding time constant of activation and steady state magnitude of I_h are consistent with the voltage clamp data of Doan and Kunze (1999). This voltage clamp study presented evidence in A-type VGN of considerable variability in activation time constants and a steady state magnitude for I_h that changed by less than a factor of two over a corresponding range of membrane potentials, i.e. those typically encountered during the plateau phase of the DVS.

Rebound excitation and the role of the steady state I_h current—Release of the hyperpolarizing step current applied to A-type VGN is often followed by the spontaneous generation of one or more AP as the membrane potential returns toward the pretest RMP (Fig. 1G, 1H, 1I). The primary action of I_h is to resist membrane hyperpolarization. This has been shown to occur through an influx of Na^+ ions should membrane potential be more positive than E_K or a combination of Na^+ and K^+ ions should membrane potential be more negative than E_K.(8) As a result, upon release of the hyperpolarizing current step there remains a net inward current which actively drives the membrane potential back toward the RMP. The greater the magnitude of I_h at the end of the hyperpolarizing current step the more

rapid will be the rate of change in membrane potential toward the pretest RMP and the more likely a spontaneous AP will be generated. This rebound excitation is akin to the well described phenomenon of "anode break excitation." Here, the hyperpolarized membrane potential reduces the percentage of voltage gated Na^+ channels in inactivated states. Return of membrane potential toward the RMP can then bring about a regenerative inward Na^+ current on account of the now greater availability of voltage gated Na^+ channels. Depending upon the rate of return of membrane potential to the RMP this regenerative inward Na^+ current may continue to grow through to spontaneous AP discharge. For A-type VGN neurons with a prominent I_h, the larger the magnitude of this inward current at the end of the hyperpolarizing current step the faster will be the rate of return to the pretest RMP along with an increased likelihood for rebound excitation. Our data support this interpretation along at least three lines of evidence (Fig. 5 and Table 1). First, as the hyperpolarizing step current magnitude increases from −70 to −120 pA, termination of the step lessens the time to the first spontaneous AP and brings about a steady reduction in the APFT (Figs. 5A and 5B). This is consistent with an increasing magnitude of I_h at the end of the more negative step currents and more negative plateau potentials for the DVS (Fig. 4, ○) bringing about a more rapid return toward the pretest RMP. The concomitant reduction in the APFT (Table 1) is a direct consequence of an elevated availability of voltage gate Na^+ channels. Second, the earlier spontaneous discharge occurs from the time of release of the hyperpolarizing current step the greater is the UV_{MAX}, peak amplitude and DV_{MAX} of the AP waveform. Again, all biophysical dynamics consistent with an increase in the availability of voltage gate Na^+ channels. Third, upon application of the HCN channel blockers ZD7288 and CsCl the DVS is completely abolished (Fig. 6B and 6D) with a peak negative membrane potential is not much different from the plateau potential at the end of the hyperpolarizing current step. The implication being that with the loss of the DVS there is a considerably more negative membrane potential at the end of the hyperpolarizing current step and very likely an even larger percentage increase in the availability of voltage gated Na^+ channels. However, upon release of the hyperpolarizing current step the HCN channel antagonists have eliminated the inward I_h and the membrane potential passively returns to the pretest membrane potential. The time course for this passive return, as opposed to the accelerated return to RMP in the presence of I_h, is long enough that a sufficient percentage of once available voltage gated Na^+ channels have time to transition to inactivated states without necessarily passing through an open ion conducting sate.(2) As a result, the percentage of voltage gate Na^+ channels available to sustain a regenerative inward Na^+ current are insufficient for continued membrane depolarization through to spontaneous AP discharge (Fig. 6B and 6D).

PEMH and the role of the steady state I_h current with increasing neuronal discharge frequency—In myelinated A-type VGN the rate of APFF increases with increasing magnitude of step depolarizing currents. Immediately upon termination of the positive step current membrane potential rapidly hyperpolarizes several millivolts below baseline before recovering to the pretest RMP (Figs. 1D, 1E and 1F, ▲). These data seemed to indicate that increasing firing rates may bring about a more pronounced post excitatory membrane hyperpolarization (PEMH). This hypothesis was substantiated in a subset of A-type VGN (n = 6) where the termination of step depolarizing currents of increasing magnitude brought about a PEMH that strongly correlated with the APFF ($r^2 = 0.979$, Fig. 3). Although application of I_h antagonists ZD7288 and CsCl eliminated the PEMH, these chemicals also eliminated sustained repetitive discharge in these cells (Fig. 6, note ▲). To more conclusively associate the PEMH with the I_h repetitive discharge would have to be induced in these cells either by a sustained high frequency burst of narrow (< 100 μsec) current pulses or repeated nerve stimulation using an intact nerve ganglion preparation.(15)

As I_h is known to contribute to RMP in A-type VGN, a PEMH implies that immediately following a period of sustained high frequency discharge the membrane hyperpolarization

may be a result of a net reduction of I_h at the pretest RMP. There are at least three plausible biophysical explanations for this interpretation. First, a leftward shift in the voltage dependent activation curve, i.e. a more negative $V_{0.5}$ would mean a smaller I_h magnitude at the pretest RMP. It has been shown that a reduction in basal levels of cAMP can lead to a negative shift in the $V_{0.5}$ of I_h by several millivolts.(5) Although additional ATP is available in the intracellular solution it may be that the sustained, elevated level of activity has transiently reduced the availability of this second messenger that is known to be intimately associated with numerous intracellular signal transduction pathways. Second, it has recently been shown that intracellular Mg^{+2} can function as a voltage-dependent blocker of HCN channels by binding to a site inside the channel pore.(20;32) These voltage clamp experiments of Lyashchenko and Tibbs (2008) and Vemana et al. (2008) suggest that such a mechanism may function to block outward HCN currents at elevated potentials and that the time constant for onset of Mg^{+2} block is on the order of 10's – 100's of microseconds, well within the time course of A-type VGN AP. The rate of Mg^{+2} unblock of the HCN channels is less clear, particularly over physiological range of membrane voltages encountered during the initial and later phases of the AP afterhyperpolarization. This would suggest that the combination of 5 mM $MgCl_2$ in the intracellular solution and the regular increases in membrane potential over the course of sustained discharge leads to an intracellular Mg^{+2} block of the HCN channels underlying the I_h current that requires several milliseconds to unblock following termination of repetitive discharge. While long in comparison to the onset time constant for Mg+2 block, the value is well within the range of time constants associated with the unblock of NMDA receptors which can range well beyond several hundred milliseconds.(11) Finally, there is an extensive literature describing a component of membrane hyperpolarization following sustained repetitive discharge that is the result of a transient deactivation of HCN channel currents and not the more widely assumed Ca^{+2}-activated K^+ currents (see(23) for discussion). While evident in olfactory, hippocampal and cholinergic interneurons such a biophysical explanation remains to be further investigated for sensory neurons of the vagal and dorsal root ganglia.

Contradictions with other studies of I_h in VGN

There is considerable consistency in the visceral and somatic sensory neuron literature that HCN1 channels are prominently expressed in myelinated A-type afferents and that the resultant I_h, which may be comprised of other HCN channel subtypes, is critically important in balancing the net transmembrane current toward a final RMP.(6;7;9;21;22;33;34) In the DRG literature, application of the HCN channel blockers ZD7288 and CsCl consistently reduces the excitability of myelinated A-type neurons to step depolarizing currents much in the same manner as observed in our experiments (Fig. 6).(9;30) Indeed, there are numerous reports from the somatic literature demonstrating that ZD7288 or HCN1 knockout can lessen mechanical allodynia and neuropathic ectopic discharge of myelinated A-type afferents.(10;13;34) In contrast, there are reports from the visceral sensory neuron literature that blockade of HCN channel currents with ZD7288 or CsCl increases the excitability of myelinated A-type VGN.(7;17) Such observations are contrary to our own data from A-type VGN and that from the general somatic sensory neuron literature. The reasons for such differences may be methodological and remain to be resolved.

Conclusions

In myelinated A-type VGN there exists a prominent inward hyperpolarization induced current, I_h, that has previously been shown to play an important role in establishing the RMP.(6) Here, we have focused upon identifying a broad spectrum of functional correlates to AP discharge with the presence of I_h and in particular the magnitude and time course of the DVS resulting from activation of I_h with hyperpolarizing step currents. Release of these

hyperpolarizing currents often leads to spontaneous AP discharge the dynamic character of which is strongly dependent upon the magnitude of the transmembrane I_h current present at the end of the current step. These data provide important foundational information concerning the natural expression of the I_h current in myelinated A-type VGN and the dynamic discharge characteristics of these cells. As evidence is growing that the HCN channel current may represent a valid target for pharmacological intervention such quantitative relationships could potentially help guide the molecular or chemical modification of HCN channel gating properties to effect a particular outcome in VGN discharge properties. Ideally, well beyond merely selective blockade of a particular HCN channel subtype.

Acknowledgments

This project was supported by research grants from the State Health (No. 2007-474) and the State Education Departments (No. 11531111) of Heilongjiang and the Chinese National Natural Science Foundation (No. 30973532) to GFQ & BYL. Partial supported was also provided by the National Institutes of Health to JHS (HL072012).

Reference List

1. Accili EA, Proenza C, Baruscotti M, DiFrancesco D. From funny current to HCN channels: 20 years of excitation. News Physiol Sci 2002;17:32–37. [PubMed: 11821534]
2. Armstrong CM. Na channel inactivation from open and closed states. Proc Natl Acad Sci U S A 2006;103:17991–17996. [PubMed: 17101981]
3. Bender RA, Brewster A, Santoro B, Ludwig A, Hofmann F, Biel M, Baram TZ. Differential and age-dependent expression of hyperpolarization-activated, cyclic nucleotide-gated cation channel isoforms 1–4 suggests evolving roles in the developing rat hippocampus. Neuroscience 2001;106:689–698. [PubMed: 11682156]
4. Dalle C, Eisenach JC. Peripheral block of the hyperpolarization-activated cation current (Ih) reduces mechanical allodynia in animal models of postoperative and neuropathic pain. Reg Anesth Pain Med 2005;30:243–248. [PubMed: 15898027]
5. Dibattista M, Mazzatenta A, Grassi F, Tirindelli R, Menini A. Hyperpolarization-activated cyclic nucleotide-gated channels in mouse vomeronasal sensory neurons. J Neurophysiol 2008;100:576–586. [PubMed: 18509074]
6. Doan TN, Kunze DL. Contribution of the hyperpolarization-activated current to the resting membrane potential of rat nodose sensory neurons. J Physiol (Lond) 1999;514(Pt 1):125–138. [PubMed: 9831721]
7. Doan TN, Stephans K, Ramirez AN, Glazebrook PA, Andresen MC, Kunze DL. Differential distribution and function of hyperpolarization-activated channels in sensory neurons and mechanosensitive fibers. J Neurosci 2004;24:3335–3343. [PubMed: 15056713]
8. Hofmann F, Biel M, Kaupp UB. International Union of Pharmacology. LI. Nomenclature and structure-function relationships of cyclic nucleotide-regulated channels. Pharmacol Rev 2005;57:455–462. [PubMed: 16382102]
9. Hogan QH, Poroli M. Hyperpolarization-activated current (I(h)) contributes to excitability of primary sensory neurons in rats. Brain Res 2008;1207:102–110. [PubMed: 18377879]
10. Jiang YQ, Xing GG, Wang SL, Tu HY, Chi YN, Li J, Liu FY, Han JS, Wan Y. Axonal accumulation of hyperpolarization-activated cyclic nucleotide-gated cation channels contributes to mechanical allodynia after peripheral nerve injury in rat. Pain 2008;137:495–506. [PubMed: 18179873]
11. Kampa BM, Clements J, Jonas P, Stuart GJ. Kinetics of Mg2+ unblock of NMDA receptors: implications for spike-timing dependent synaptic plasticity. J Physiol 2004;556:337–345. [PubMed: 14754998]
12. Kitagawa J, Takeda M, Suzuki I, Kadoi J, Tsuboi Y, Honda K, Matsumoto S, Nakagawa H, Tanabe A, Iwata K. Mechanisms involved in modulation of trigeminal primary afferent activity in rats with peripheral mononeuropathy. Eur J Neurosci 2006;24:1976–1986. [PubMed: 17040479]

13. Lee DH, Chang L, Sorkin LS, Chaplan SR. Hyperpolarization-activated, cation-nonselective, cyclic nucleotide-modulated channel blockade alleviates mechanical allodynia and suppresses ectopic discharge in spinal nerve ligated rats. J Pain 2005;6:417–424. [PubMed: 15993819]
14. Li BY, Qiao GF, Feng B, Zhao RB, Lu YJ, Schild JH. Electrophysiological and neuroanatomical evidence of sexual dimorphism in aortic baroreceptor and vagal afferents in rat. Am J Physiol Comp Integ Physiol 2008;295:1301–1310.
15. Li BY, Schild JH. Patch clamp electrophysiology in nodose ganglia of adult rat. Journal of Neuroscience Methods 2002;115:157–167. [PubMed: 11992667]
16. Li BY, Schild JH. Electrophysiological and pharmacological validation of vagal afferent fiber type of neurons enzymatically isolated from rat nodose ganglia. J Neurosci Methods 2007;164:75–85. [PubMed: 17512602]
17. Li YL, Tran TP, Muelleman R, Schultz HD. Blunted excitability of aortic baroreceptor neurons in diabetic rats: involvement of hyperpolarization-activated channel. Cardiovasc Res 2008;79:715–721. [PubMed: 18524809]
18. Ludwig A, Budde T, Stieber J, Moosmang S, Wahl C, Holthoff K, Langebartels A, Wotjak C, Munsch T, Zong X, Feil S, Feil R, Lancel M, Chien KR, Konnerth A, Pape HC, Biel M, Hofmann F. Absence epilepsy and sinus dysrhythmia in mice lacking the pacemaker channel HCN2. EMBO J 2003;22:216–224. [PubMed: 12514127]
19. Ludwig A, Zong X, Jeglitsch M, Hofmann F, Biel M. A family of hyperpolarization-activated mammalian cation channels. Nature 1998;393:587–591. [PubMed: 9634236]
20. Lyashchenko AK, Tibbs GR. Ion binding in the open HCN pacemaker channel pore: fast mechanisms to shape "slow" channels. J Gen Physiol 2008;131:227–243. [PubMed: 18270171]
21. Masuda N, Hayashi Y, Matsuyoshi H, Chancellor MB, de Groat WC, Yoshimura N. Characterization of hyperpolarization-activated current (Ih) in dorsal root ganglion neurons innervating rat urinary bladder. Brain Res 2006;1096:40–52. [PubMed: 16765328]
22. Momin A, Cadiou H, Mason A, McNaughton PA. Role of the hyperpolarization-activated current Ih in somatosensory neurons. J Physiol 2008;586:5911–5929. [PubMed: 18936078]
23. Oswald MJ, Oorschot DE, Schulz JM, Lipski J, Reynolds JN. IH current generates the afterhyperpolarisation following activation of subthreshold cortical synaptic inputs to striatal cholinergic interneurons. J Physiol 2009;587:5879–5897. [PubMed: 19884321]
24. Qiao GF, Li BY, Lu YJ, Fu YL, Schild JH. 17Beta-estradiol restores excitability of a sexually dimorphic subset of myelinated vagal afferents in ovariectomized rats. Am J Physiol Cell Physiol 2009;297:C654–C664. [PubMed: 19570896]
25. Santoro B, Baram TZ. The multiple personalities of h-channels. Trends Neurosci 2003;26:550–554. [PubMed: 14522148]
26. Schild, JH.; Alfrey, KD.; Li, BY. Voltage-gated ion channels in vagal afferent neurons. In: Undem, BJ.; Weinreich, D., editors. Advances in Vagal Afferent Neurobiology. CRC; 2005. p. 77-100.
27. Schild JH, Clark JW, Hay M, Mendelowitz D, Andresen MC, Kunze DL. A- and C-type rat nodose sensory neurons: model interpretations of dynamic discharge characteristics. J Neurophysiol 1994;71:2338–2358. [PubMed: 7523613]
28. Schild JH, Kunze DL. Experimental and modeling study of Na+ current heterogeneity in rat nodose neurons and its impact on neuronal discharge. J Neurophysiol 1997;78:3198–3209. [PubMed: 9405539]
29. Tompkins JD, Lawrence YT, Parsons RL. Enhancement of Ih, but not inhibition of IM, is a key mechanism underlying the PACAP-induced increase in excitability of guinea pig intrinsic cardiac neurons. Am J Physiol Regul Integr Comp Physiol 2009;297:R52–R59. [PubMed: 19403861]
30. Tu H, Deng L, Sun Q, Yao L, Han JS, Wan Y. Hyperpolarization-activated, cyclic nucleotide-gated cation channels: roles in the differential electrophysiological properties of rat primary afferent neurons. J Neurosci Res 2004;76:713–722. [PubMed: 15139030]
31. Tu H, Zhang L, Tran TP, Muelleman RL, Li YL. Diabetes alters protein expression of hyperpolarization-activated cyclic nucleotide-gated channel subunits in rat nodose ganglion cells. Neuroscience 2010;165:39–52. [PubMed: 19815055]
32. Vemana S, Pandey S, Larsson HP. Intracellular Mg2+ is a voltage-dependent pore blocker of HCN channels. Am J Physiol Cell Physiol 2008;295:C557–C565. [PubMed: 18579800]

33. Wan Y. Involvement of hyperpolarization-activated, cyclic nucleotide-gated cation channels in dorsal root ganglion in neuropathic pain. Sheng Li Xue Bao 2008;60:579–580. [PubMed: 18958363]

34. Wickenden AD, Maher MP, Chaplan SR. HCN pacemaker channels and pain: a drug discovery perspective. Curr Pharm Des 2009;15:2149–2168. [PubMed: 19519450]

35. Zagotta WN, Olivier NB, Black KD, Young EC, Olson R, Gouaux E. Structural basis for modulation and agonist specificity of HCN pacemaker channels. Nature 2003;425:200–205. [PubMed: 12968185]

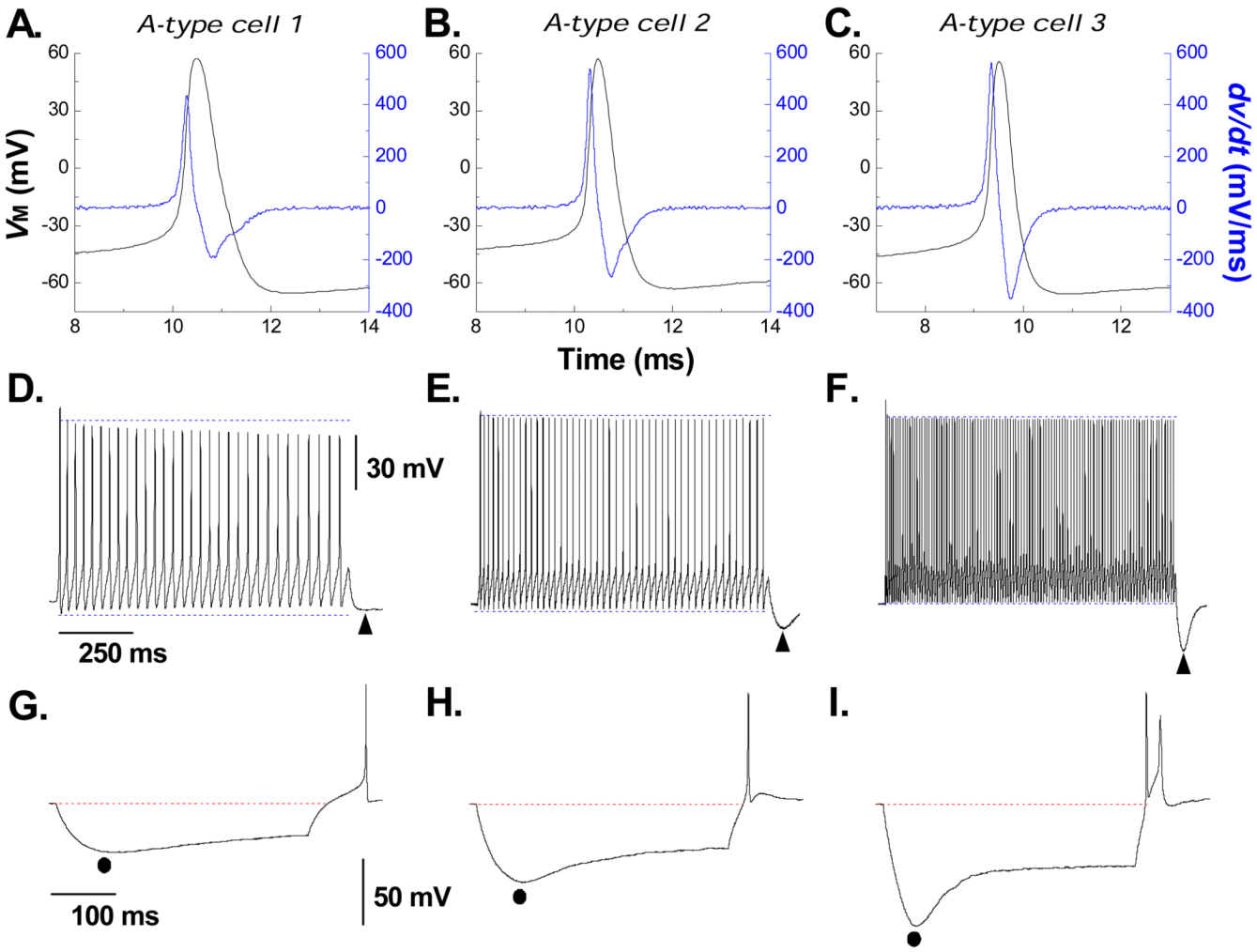

Figure 1. Myelinated A-type vagal neurons express varying levels of cell excitability and hyperpolarization-induced depolarizing voltage sag

Three distinct examples from a population (n = 47) of myelinated A-type vagal neuron (VGN) implicating that increased cell excitability generally presents with an increased magnitude and time course of hyperpolarization-induced depolarization voltage sag (DVS). **A)** Single action potential (AP, black trace) evoked by a brief current pulse along with the corresponding *dv/dt* (blue trace). **B)** Sustained repetitive AP discharge in response to a 1000 msec, 150 pA current step. Immediately upon termination of the step a period of post excitatory membrane hyperpolarization was observed (PEMH, ▲). **C)** In response to a 400 msec, −120 pA current pulse membrane potential reached a peak hyperpolarization (●) followed by a depolarizing voltage sag (DVS). Immediately upon termination of the hyperpolarizing step current the trajectory of membrane potential back toward the RMP often elicited an AP. Protocols were the same for the two other example VGN (**D – F** and **G – H**) but with a clear trend toward an increased excitability revealing a more prominent magnitude and time course of the PEMH, peak hyperpolarization and DVS.

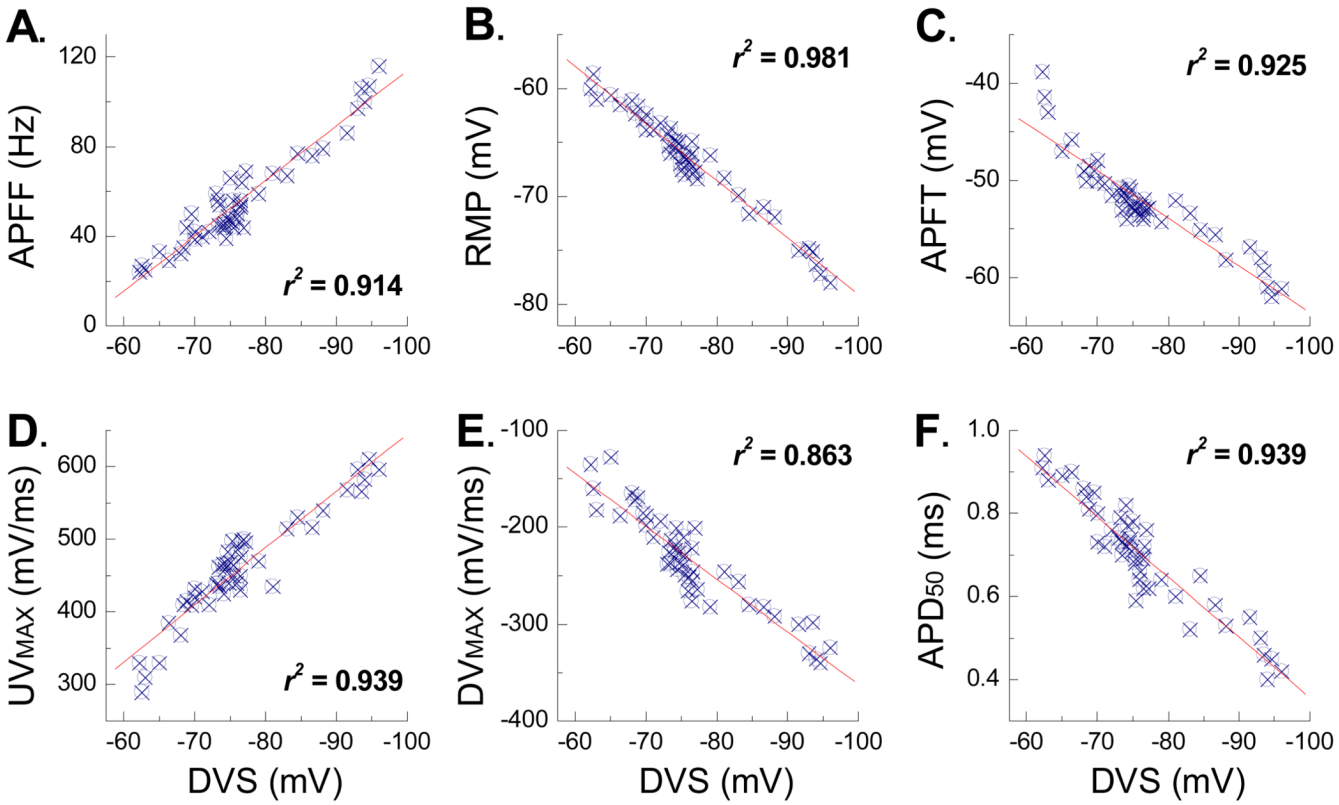

Figure 2. Depolarizing voltage sag (DVS) and the excitability characteristics of A-type VGN

Six functionally distinct measures of membrane excitability from VGN identified as myelinated A-type (n = 47) were correlated with the peak magnitude of the DVS elicited in response to a −120 pA current step. **A)** AP firing frequency (APFF), **B)** resting membrane potential (RMP), **C)** AP firing threshold (APFT), **D)** maximum AP upstroke velocity (UV_{MAX}), **E)** maximum AP down stroke velocity (DV_{MAX}), and **F)** AP duration (APD_{50}). Each measure was acquired from each of the A-type VGN under study. The square of the Pearson product moment correlation coefficient (r^2) and linear trend lines were generated using Excel.

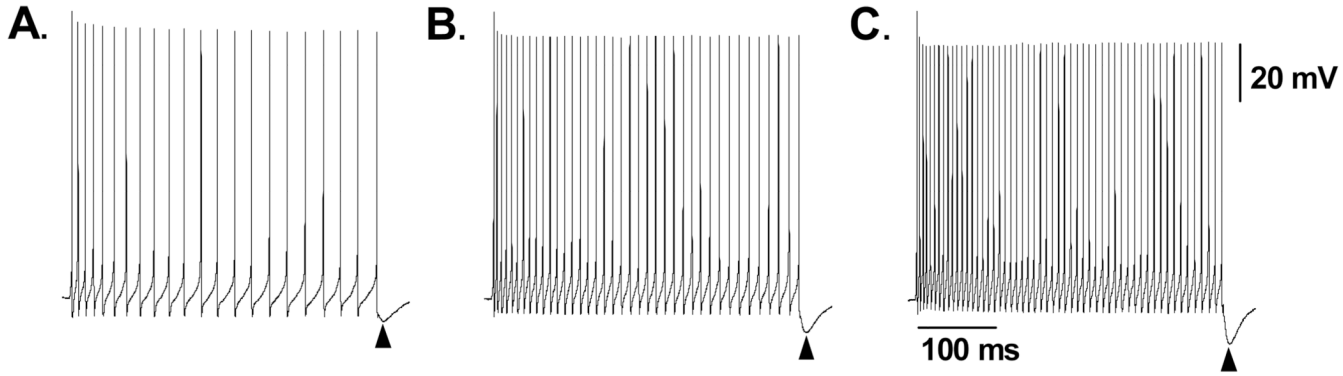

Figure 3. Discharge frequency and post excitatory membrane hyperpolarization in A-type VGN

In a subset of myelinated A-type VGN (n = 6) repetitive AP discharge was elicited by three successive 400 msec depolarizing step currents of **A)** 50 pA, **B)** 100 pA and **C)** 150 pA. The peak magnitude and time course of the post excitatory membrane hyperpolarization (PEMH, note ▲ upon termination of the step current) tended to increase along with increased discharge rates at higher stimulus currents. The peak PEMH was found to be strongly correlated with the steady state APFF ($r^2 = 0.979$).

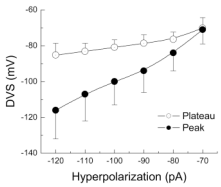

Figure 4. Current-voltage profile of the DVS in A-type VGN

In a subset of myelinated A-type VGN (n = 6) the peak (●) and plateau (○) membrane potentials were measured in response to 400 msec hyperpolarizing current steps from RMP and presented as an average current-voltage plot (IV). Despite substantial membrane hyperpolarization near the start of the current pulse, the DVS plateaued to membrane potentials within a range of ~10 mV.

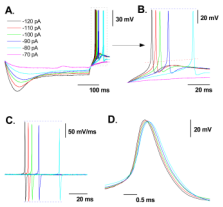

Figure 5. Magnitude of DVS impacts the trajectory of rebound membrane depolarization

In a subset of myelinated A-type VGN (n = 6) **A)** 400 msec hyperpolarizing current steps of −70 to −120 pA in magnitude from RMP brought about an ever increasing magnitude and time course of DVS. **B)** Upon release of the hyperpolarizing current membrane potential rebounded toward the starting RMP which often led to spontaneous generation of one or more AP. **C)** The peak magnitude of the AP time derivative was inversely related to the time delay between release of the hyperpolarizing current and the measured APFT for spontaneous AP discharge. **D)** Registration of the spontaneous AP according to the time of APFT. See Table 1 for comparison of measures of AP wave shape as a function of DVS magnitude and time course.

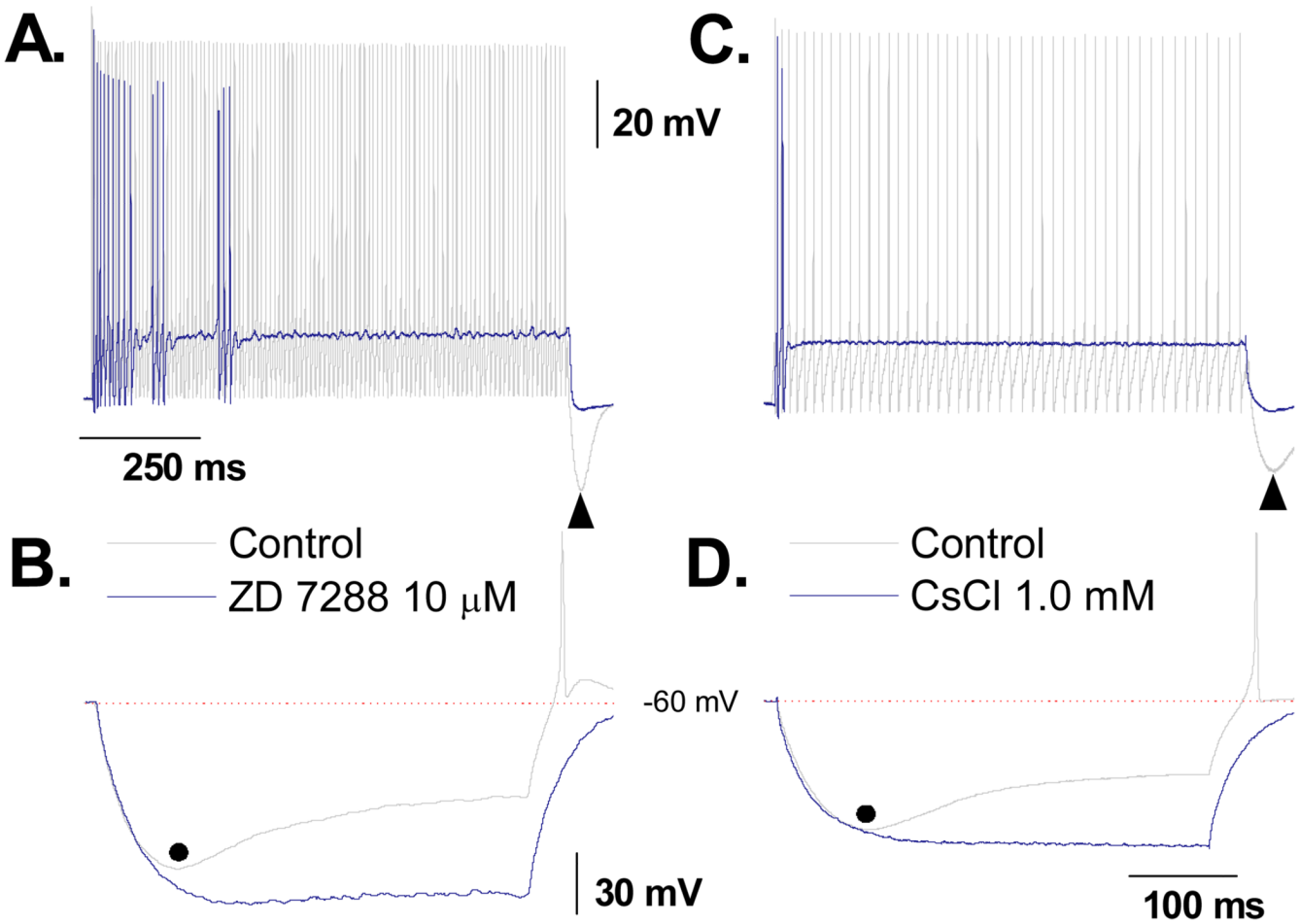

Figure 6. Impact of ZD7288 and CsCl on DVS and excitability of A-type VGN

In a subset of A-type VGN (n = 5), **A)** a 1000 msec, 150 pA step current under control conditions consistently elicited sustained repetitive discharge. Following bath application of 10 μM ZD7288 cell excitability was substantially reduced, often presenting as irregular, shirt duration AP bursts. **B)** Prior to application of the HCN channel antagonist a 400 msec, −120 pA step current brought about a characteristic DVS response along with generation of spontaneous AP(s) upon release of the hyperpolarizing current step. Consistent with loss of the HCN channel current these characteristics were abolished in the presence of 10 μM ZD7288. These same protocols were repeated in a subset of A-type VGN (n = 5) but with 1 mM CsCl substituted as the HCN channel antagonist **(C and D)** and comparable effects were observed.

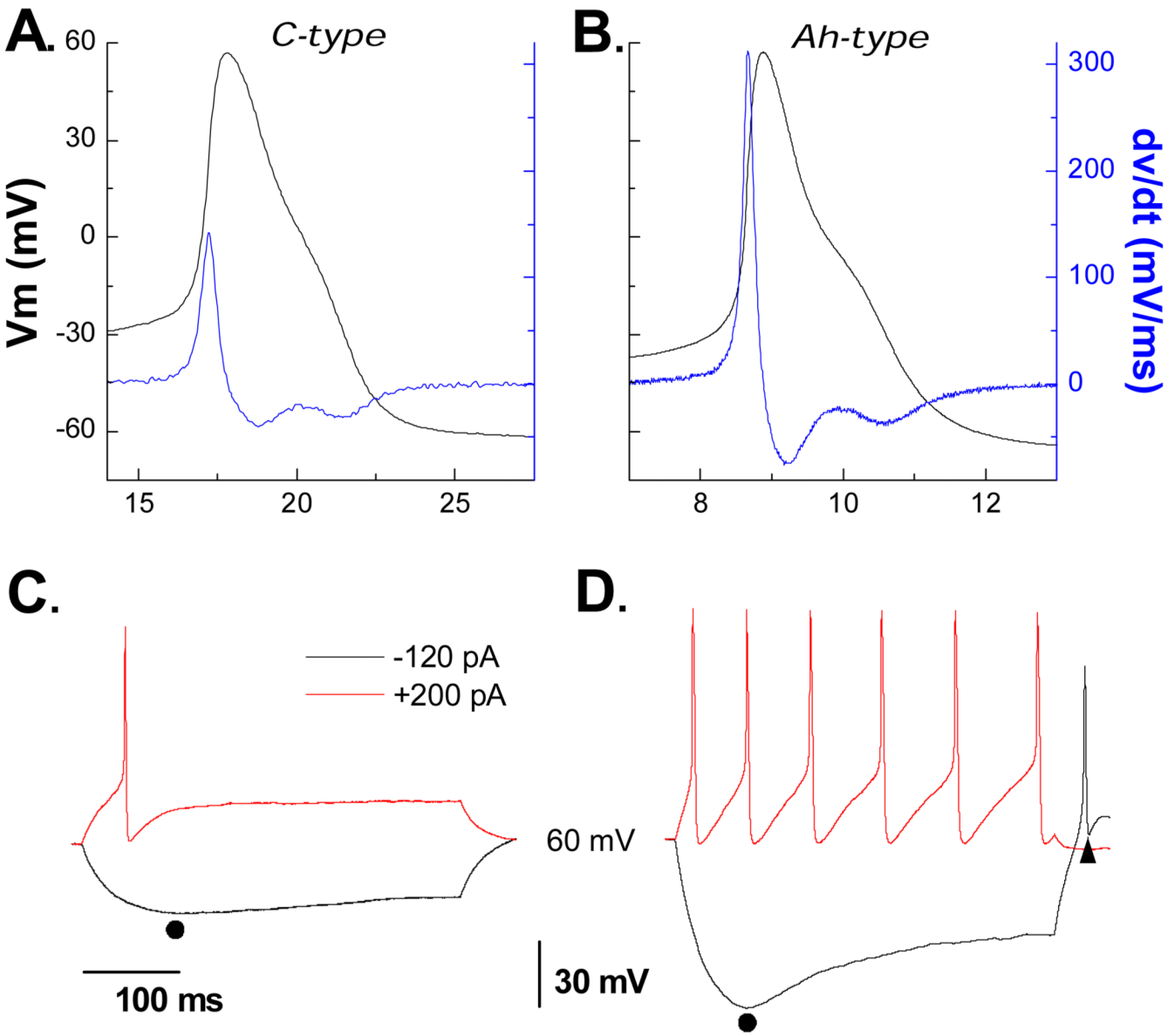

Figure 7. Contrasting dynamics of DVS, PEMH and rebound excitation in Ah- and C-type VGN

A) In a small cohort of female rats a subset of VGN were identified as myelinated Ah-type (n = 5). **B)** These cells exhibited all the functional characteristics of an I_h current as observed in myelinated A-type VGN in particular a prominent DVS, PEMH and spontaneous discharge following release of a hyperpolarizing current step. **C and D)** In contrast, VGN identified as C-type (n = 22) were far less excitable and exhibited none of the functional characteristics of an I_h current.

Table 1

Measures of A-type VGN wave shape characteristics as a function of the peak magnitude and time course of a hyperpolarizing current induced depolarizing voltage sag (DVS).

Parameter	**400 msec hyperpolarizing current step**					
Step magnitude	**−120 pA**	**−110 pA**	**−100 pA**	**−90 pA**	**−80 pA**	**r^2**
DVS peak (mV)	159 ± 21	147 ± 17	136 ± 15	125 ± 21	112 ± 14	0.948
Slope factor	19 ± 5	21 ± 8	23 ± 7	26 ± 8	31 ± 9	0.992
APFT (mV)	−46 ± 3	−45 ± 3	−44 ± 3	−42 ± 3	−40 ± 3	0.989
UV_{MAX} (mV/ms)	360 ± 85	355 ± 78	348 ± 74	338 ± 77	327 ± 68	0.977
DV_{MAX} (mV/ms)	178 ± 44	−175 ± 46	−170 ± 39	−162 ± 43	−155 ± 32	0.962
APD_{50} (ms)	0.78 ± 0.11	0.82 ± 0.08	0.86 ± 0.10	0.89 ± 0.08	0.93 ± 0.11	0.986

Data expressed as mean ± SD (n = 6 myelinated A-type VGN). **DVS:** hyperpolarizing current-induced depolarizing voltage sag; **Slope factor:** trajectory of DVS dependent rebound membrane depolarization; **APFT:** action potential firing threshold; **UV_{MAX}:** maximum AP upstroke velocity; **DV_{MAX}:** maximum down stroke velocity; **APD_{50}:** AP duration as measured at 50% of the peak-to-peak AP excursion.